SATELLITE- AND GROUND-BASED MULTI-VIEW PHOTOGRAMMETRIC DETERMINATION OF 3D CLOUD GEOMETRY

G. Seiz*, D. Poli, A. Gruen, E. P. Baltsavias, A. Roditakis

Institute of Geodesy and Photogrammetry, Swiss Federal Institute of Technology (ETH) Zurich
ETH Hoenggerberg, CH-8093 Zurich, Switzerland
{gseiz, daniela, agruen, manos, roditak}@geod.baug.ethz.ch

Commission VII, WG VII/6

KEY WORDS: Atmosphere, Global Change, Sensor Orientation, Matching, Camera, Visualization.

ABSTRACT:

The quantitative 3D description of clouds is important for refined methods in nowcasting and the modeling of weather and climate. The EU project Cloudmap aimed at developing new methodologies for cloud product derivation (heights, type, optical thickness and effective droplet size). The follow-up project Cloudmap2 aimed at producing and exploiting value-added remote sensing data products on macroscopic (e.g. cloud-top height) and microscopic (e.g. cloud droplet radius) properties and water vapour distributions in order to characterize sub-grid scale processes within Numerical Weather Prediction Models (NWP) through validation and data assimilation.

Earth Observation (EO) image data, provided by ESA, EUMETSAT and NASA are used to derive geophysical value-added data products over Europe and the North Atlantic region, whenever possible in near real-time. Ground-based active (cloud radar, ceilometer) and passive (stereo imager system, IR camera) remote-sensing instruments are used to validate the EO-derived products as well as to merge them with the satellite-based results for a full 3D representation of the clouds. The role of our group in Cloudmap2 was to estimate cloud-top height (CTH) and wind (CTW) from stereo images from satellites and cloud-bottom height (CBH) and wind (CBW) from stereo images acquired by our newly developed ground-based stereo imager system. The cloud-top and -bottom results were then combined into a 3D model and visualized. This paper describes the results obtained in CTH and CTW estimation from ATSR2, AATSR, MISR and Meteosat-6/-7, including validation, the CBH and CBW results from the ground-based stereo imager system and a case study where the satellite- and ground-based 3D cloud boundary results are combined.

1. INTRODUCTION

The interest to monitor cloud properties from space and ground-based observations is based on the large influence that clouds have on the Earth and Atmosphere energy balance. The EU-FP4 project Cloudmap aimed at estimating new cloud-top products (heights, type, optical thickness, effective droplet size), especially for cirrus and contrail clouds from existing and new sensors, using three different techniques (brightness temperature with CO2 slicing method, stereoscopy and Oxygen A-band). These cloud-top products have been validated using airborne sensor underflights, multi-resolution observations from space sensors and ground-based remote sensing instruments. Cloudmap ended in January 2001 and was then continued by the EU-FP5 project Cloudmap2 (www-research.ge.ucl.ac.uk/cloudmap2/) until June 2004.

Cloudmap2 aimed at producing and exploiting value-added remote sensing data products on macroscopic (e.g. cloud-top height) and microscopic (e.g. cloud droplet radius) properties and water vapour distributions in order to characterize sub-grid scale processes within Numerical Weather Prediction Models (NWP) through validation and data assimilation. Earth Observation (EO) data, provided by ESA, EUMETSAT and NASA are used to derive geophysical value-added data products over Europe and the North Atlantic region, whenever possible in near real-time. Ground-based active (cloud radar, ceilometer) and passive (stereo imager system, IR camera) remote sensing instruments are used to validate the EO-derived products as well as to be merged with the satellite-based results for a whole 3D representation of the clouds. Numerical simulation experiments based on state-of-the-art radiative transfer methods are used to quantify the effect of broken clouds on the Earth's radiation budget and lead to a better representation of clouds within NWP models.

The role of our group in Cloudmap and Cloudmap2 was to estimate cloud-top height (CTH) and wind (CTW) from stereo images from satellites and cloud-base height (CBH) and wind (CBW) from stereo images acquired by our own ground-based stereo imager system, with stereo-photogrammetric techniques. As second step, the cloud-top and -base results were then combined and visualized in 3D.

This paper describes the CTH and CTW retrieval from multi-view satellite sensors (ATSR2/AATSR, MISR) and geostationary satellites (Meteosat-6/-7) and the comparison/validation of these cloud products with other satellite-based products as well as measurements from ground-based instruments (multi-camera system, cloud radar). Finally, a case study is presented where the satellite- and ground-based 3D cloud boundary results were combined.

* Corresponding author.

2. SATELLITE-BASED STEREO ANALYSIS

The satellite-based stereo analysis includes several processing steps which are illustrated in Figure 1. After the data description in Section 2.1, the sensor model for image georeferencing will be presented in Section 2.2. The subsequent processing steps are explained in Section 2.3.

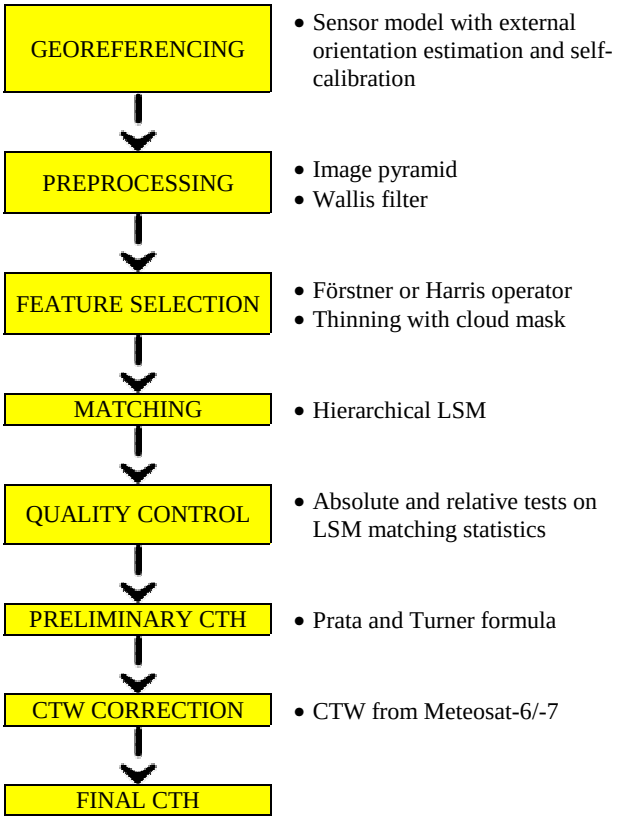

Figure 1. Schematic overview of stereo-photogrammetric processing of the satellite-based images to derive CTH and CTW.

2.1 Data

2.1.1 ATSR2 / AATSR: The Along Track Scanning Radiometer (ATSR2) instrument is part of the ERS-2 satellite system which was launched in April 1995. The successor sensor, AATSR, is part of Envisat, which was launched in Spring 2002. ERS-2 and Envisat are in a near-circular, sun-synchronous orbit at a mean height of 780 km, an inclination of 98.5° and a sub-satellite velocity of 6.7 km/s. The repeat cycle of ATSR2/AATSR is approximately 3 days.

The ATSR2/AATSR sensor first views the surface along the direction of the orbit track at an incidence angle of 55° as it flies toward the scene. Then, some 120 s later, ATSR2 records a second observation of the scene at an angle close to the nadir. The ATSR2 field of view is comprised of two 500 km-wide curved swaths with 555 pixels across the nadir swath and 371 pixels across the forward swath. The pixel size is 1 km x 1 km at the center of the nadir scan and 1.5 km x 2 km at the center of the forward scan. The sensor records in seven spectral channels, i.e. 0.55 µm, 0.67 µm, 0.87 µm, 1.6 µm, 3.7 µm, 10.8 µm and 12.0 µm. All channels have a radiometric resolution of 10-bit. Our CTH retrieval is based on the rectified data products, GBT for ATSR2 and ATS_TOA_1P for AATSR. The geolocation of these rectified products is achieved by mapping the acquired pixels onto a 512 x 512 grid with 1 km pixel size whose axes are the satellite ground-track and great circles orthogonal to the ground-track.

2.1.2 MISR: The Multi-angle Imaging SpectroRadiometer (MISR) is currently the only operational satellite that acquires images from nine different viewing angles. MISR was launched on board the EOS AM-1 Terra spacecraft in December 1999. The orbit is sun-synchronous at a mean height of 705 km with an inclination of 98.5° and an equatorial crossing time of about 10:30 local solar time. The repeat cycle is 16 days. The MISR instrument consists of nine pushbroom cameras at different viewing angles: -70.5° (named DA), -60.0° (CA), -45.6° (BA), -26.1° (AA), 0.0° (AN), 26.1° (AF), 45.6° (BF), 60.0° (CF), and 70.5° (DF). The time delay between adjacent camera views is 45-60 seconds, which results in a total delay between the DA and DF images of about 7 minutes. The four MISR spectral bands are centered at 446 nm (blue), 558 nm (green), 672 nm (red) and 866 nm (NIR). The red-band data from all nine cameras and all spectral bands of the nadir camera are saved in high-resolution with a pixel size of 275 m x 275 m. The data of the blue, green and NIR bands of the remaining eight non-nadir cameras are stored in low-resolution with a pixel size of 1.1 km x 1.1 km. The operational data products from MISR are described in (Lewicki et al., 1999). The two products used for this study are the L1B1 radiance and the L1B2 ellipsoid-projected radiance data.

The L1B1 product is radiometrically but not geometrically corrected, while the L1B2 ellipsoid-projected radiance product is referenced to the surface of the WGS84 ellipsoid with no terrain elevation included. The MISR georectified product spatial horizontal accuracy requirements are driven by the needs of the geophysical parameter retrieval algorithms. The goal of operational MISR data processing is to achieve an uncertainty better than ± 140 m for both the absolute geolocation of the nadir camera and the co-registration between all nine cameras (Jovanovic et al., 2002). The latest evaluation results of the L1B2 geolocation accuracy as shown in (Jovanovic et al., 2004) are approaching prelaunch requirements, with along- and cross-track errors far below 1 pixel for all cameras (except DA).

The operational L2TC top-of-atmosphere/ cloud product, which contains the operationally derived cloud parameters, like stereo CTH, east-west (EW) and north-south (NS) cloud motion components, as well as many additional parameters from the stereo retrieval (Diner et al., 2001), can be used as comparison data for validation (Seiz, 2003).

2.2 Sensor Modeling

The aim of rigorous sensor models is to establish a relationship between image and ground reference systems according to the sensor geometry of acquisition. In particular, different approaches have been proposed for the georeferencing of pushbroom sensors carried on aircraft (Gruen et al., 2002) and satellite (Poli, 2003). A flexible sensor model that can be applied to a wide class of linear CCD array sensors has been developed in our group and already applied to different linear scanners carried on satellite and aircraft (Poli, 2003). The model is based on the photogrammetric collinearity equations, that are extended in order to include the external orientation modeling with 2nd order piecewise polynomials and a self-calibration for the correction of lens distortions and CCD lines rotations in the focal plane.

The sensor model was applied to georeference the MISR level 1B1 product (Poli, 2003). Two areas of interest, over Germany and South France, were chosen. From the test over Germany a GCP accuracy of 173 m in X, 87 m in Y and 80 m in Z was achieved, corresponding to 0.6, 0.3 and 0.3 pixels (ground pixel size: 275m). For the test over South France, RMS errors of 43 m in X, 45 m in Y and 152 m in Z, corresponding to 0.2, 0.2 and 0.6 pixels, were obtained.

The first results are promising, because the images have been oriented with sub-pixel accuracy. The self-calibration was fundamental because it allowed the estimation of the correct internal and external orientation parameters. In these tests, significant values for the principal point displacement have been estimated. Without self-calibration, the RMS errors in GCPs were larger than one pixel.

All of our MISR CTH and CTW calculations presented in this study (Section 2.3) fully rely on the operational L1B2 georectified radiance data. In the future, however, it is planned to use the georectification from the described in-house sensor model.

2.3 Cloud-Top Height and Motion Estimation

Determination of CTH from ATSR2, AATSR or any two views of MISR proceeds along the same scheme, as illustrated in Figure 1. First, all images were reduced to 8-bit with linear stretching between the minimum and maximum values. As no a-priori values of the cloud heights were given to the matching algorithm, the number of pyramid levels for the hierarchical matching was chosen so that the maximum possible parallax at the highest level was only 1-2 pixels. Three and five pyramid levels were used for ATSR2/AATSR and MISR, respectively. Every pyramid level was enhanced and radiometrically equalized with the Wallis filter. According to the block or filter size, different cloud structures could be enhanced. In general, a block size of about 70 pixels was chosen at the original level, which was then decreased up the pyramid. Points with good texture were selected with the Förstner or Harris interest operator in the first or second pyramid level because it is likely that these same points are readily detectable in the other levels. If a cloud mask was available (e.g. our own cloud mask for ATSR2, L1 RCCM or L2TC cloud masks for MISR), we used it for thinning of the point set to cloud points only, prior to matching.

The unconstrained Multi-Photo Geometrically Constrained (MPGC) least-squares matching (LSM) (Gruen, 1985; Baltsavias, 1991) was applied hierarchically, starting on the highest pyramid level. After each pyramid level, quality control with absolute tests on the LSM matching statistics was performed to exclude the largest blunders from further processing down the pyramid. The patch size was slightly increased from one pyramid level to the next, from 7 x 7 on the highest level to about 15 x 15 on the lowest level.

After applying the MPGC LSM algorithm, the matching solutions were quality-controlled with absolute and relative tests on the matching statistics. Additionally, meteorological criteria can be used in the detection of large blunders, including minimum and maximum cloud heights, minimum and maximum cross-track parallaxes, which are, after division by the time difference, proportional to the cross-track wind speed, or filtering the cloud heights with the brightness temperature values from the IR channel(s) in the case of ATSR2/AATSR.

The resulting y-parallaxes were converted into cloud-top heights according to Prata and Turner (1997). The zenith angles (e.g. θ_{nadir} and $\theta_{forward}$ for ATSR2/AATSR) thereby had to be projected on the along-track plane. The height values of the successfully matched points were finally interpolated to the full resolution grid.

The accuracy of the retrieved cloud-top heights was dependent on the geometric stereo configuration expressed as the base-to-height ratio B/H, the matching accuracy Δy_p, the accuracy of the georectification, including the exact values of the zenith angles, and the along-track motion retrieval accuracy $\Delta v'$. In Table 1 the B/H values and image time differences for ATSR2/AATSR and three different viewing angle combinations of MISR are listed, together with an estimation of the height error Δh given an along-track parallax error Δy_p of 1 pixel from matching or an along-track motion error $\Delta v'$ of 5 m/s.

For all sensors, the height error due to motion errors is very prominent. In contrast to stereo image pairs from scan-synchronized geostationary satellites, stereo image pairs from a single polar-orbiting satellite are never perfectly synchronous. There is a time delay of seconds to minutes between image acquisition at the different viewing angles. The resulting errors in stereo cloud-top height retrievals can be quite large, depending on the along-track cloud motion, as pointed out in Table 1. If more than two non-symmetric views are available, the along-track parallax can be separated into the amount due to cloud height and the amount due to cloud motion. With only two views, or symmetric multiple views, which is the usual case, the along-track cloud motion has to be corrected with data from an independent source. One possible source of independent data is geostationary satellite cloud motion information. In our study, three types of geostationary data from the two European satellites Meteosat-6 and Meteosat-7 (Eumetsat, 2003) were used: the Meteosat-6 5-minute Rapid Scans during MAP, the quasi-operational Meteosat-6 10-minute Rapid Scans and the operational Meteosat-7 30-minute sequences. The launch of the first Meteosat Second Generation (MSG) satellite (called Meteosat-8 since its transition into operational mode in March 2004) in August 2002, with a temporal resolution of 15 minutes, now offers a further data source for accurate CTW retrieval in several spectral bands.

Sensor	B/H ratio	Δt [s]	Δh [m] for Δy_p = 1 pixel	Δh [m] for $\Delta v'$ = 5 m/s
ATSR2/ AATSR	0.7-1.2	100-130	830-1430	420-930
MISR AN-AF	0.49	45	560	460
MISR AN-BF	1.02	92	270	450
MISR AN-DF	2.85	204	95	360

Table 1. Height error caused by parallax error and along-track motion for various B/H and time acquisition difference cases.

For cross-track wind retrieval and along-track wind correction, the exact time difference Δt between corresponding pixels in the forward and nadir scans had to be calculated. For ATSR2/AATSR, the time difference varies significantly over

the scan and can be calculated from the along-track distance on the ground and the satellite velocity after Lorenz (1985). For MISR, the time difference for different cross-track positions within a block or scene can be assumed as constant. Northerly winds lead to an underestimation of the heights and the along-track wind component has to be added to the y-parallax, while southerly winds result in overestimation of cloud-top heights. The motion vectors retrieved from Meteosat-6 and Meteosat-7 data were resampled to the ATSR2 or MISR grid and the cross- and along-track wind components calculated. Using the time difference between the acquisition of the two views, the along-track wind components were converted into CTH corrections.

3. VALIDATION

As each observation and each retrieval method have its own characteristics, much can be learned from a intercomparison of the results. The objective is to document the relative performance of the different observations of cloud top height, and where possible to understand this. In collaboration with Eumetsat and the Rutherford Appleton Laboratory (RAL), two case studies were analyzed with spaceborne observations from ATSR2, MISR and Meteosat-6/-7 and ground-based observations by the Chilbolton radar and radiosondes. The results are summarized in Table 2; the retrieval methodologies (next to our stereo processing) are described in detail in Tjemkes et al. (2002).

Date	ATSR2	MISR	Radar	Radiosonde
28/06/2000	2.3 ± 0.2	2.4 ± 0.2	2.48 ± 0.03	2.5 ± 0.2
13/06/2001	4.5 ± 0.3	4.4 ± 0.2	4.27 ± 0.08	4.6 ± 0.2

Table 2. CTH results (in km above sea-level) from ATSR2, MISR, radar and radiosondes for two cases (20 June 2000 and 13 June 2001) over Chilbolton, UK.

Based on the validation experience from Cloudmap2, a new comparison study of cloud height assignment methods has been started by Eumetsat in November 2003. Next to the multi-view photogrammetric retrieval from MISR and AATSR, the cloud height will be determined by optimal estimation from AATSR (by RAL), CO_2 slicing from MODIS and Oxygen A-band from MERIS (by Free University Berlin). The comparison of these different height products with the operational Eumetsat AMV (Atmospheric Motion Vector) product will allow to evaluate the strengths and weaknesses of each individual height assignment method within the AMV production chain. Results from Phase 1 of the study are reported in Fischer et al. (2004).

4. COMBINATION WITH GROUND-BASED STEREO DATA

For the acquisition of ground-based stereo images of clouds, a camera imager system has been developed (Figure 2). The system, data acquisition and data processing is described in detail in Seiz et al. (2002). The imager system was part of the MAP-Special Observation Period (SOP) composite observing system at the Rhine Valley, Switzerland, in autumn 1999 and was later installed at the Zürich-Kloten airport in September 2001 and April 2002. The system was used for the retrieval of cloud-bottom heights, which were then used for the validation of stereo cloud-top heights of vertically thin clouds (e.g. cirrus, contrails) and for the combination of cloud-bottom boundaries with satellite-derived cloud-top boundaries for a 3D representation of the current cloud field. This second application is explained in the next section.

Figure 2. Ground-based imager system (Skycam).

4.1 Combination of Satellite- and Ground-based Datasets

For assimilation experiments with a very high-resolution version of the operational NWP model at MeteoSwiss, several Skycam measurements series were performed at Zurich-Kloten airport in April 2002, in coincidence with satellite (ASTER, MISR) overpasses. In collaboration with the German Aerospace Center (DLR), a 3D cloud data set was then derived from the combination of MISR stereo cloud-top heights, MODIS microphysical data and Skycam stereo cloud-bottom heights. On a 50 m x 50 m grid, the cloud geometry was defined by the cloud mask and the cloud-bottom heights from Skycam and by the cloud-top heights from MISR. According to the effective radius reached close to the cloud top and the total optical thickness (both from MODIS MOD06 data), a constant liquid water gain and a droplet number density could be derived for each cloudy column. Thus, an internal profile of microphysics of a vertical resolution of 50 m was achieved (Figure 3). More details about the 3D cloud boundary extraction and subsequent application in radiative transfer simulations at DLR can be found in Seiz (2003) and in the Cloudmap2 Final Report, D13/D14 (Cloudmap2, 2004).

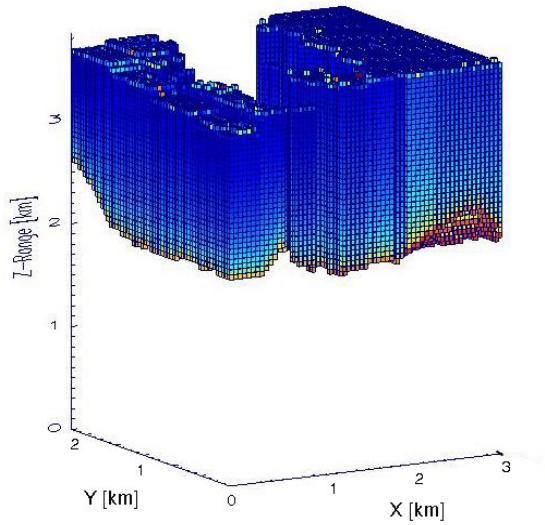

Figure 3. 3D cloud water distribution, derived from 3D cloud boundary data (MISR, ground-based camera system) and MODIS information, 19 April 2002 (image courtesy: Tobias Zinner, DLR).

5. CONCLUSIONS

This paper has shown examples of satellite- and ground-based stereo analysis of clouds. Regarding satellites, there are various sensors currently available which can be used for stereo-photogrammetric cloud retrievals. For stereo CTHs from a single polar-orbiter with only two viewing angles (e.g. ATSR2), it has been proven to be absolutely necessary to correct the preliminary heights with cloud-top wind (CTW) data from another source. Over land and mountainous regions, the cloud motion is most accurately derived from simultaneous images of a geostationary satellite. Over Europe, the Meteosat-6 Rapid Scan trials in 1999 (5min) and in 2000 (10min), and the operational Meteosat-6 10min Rapid Scans (since September 2001) are perfectly suited for this objective. The MISR instrument and its products were presented as a promising alternative to derive CTH and CTW simultaneously with stereo-photogrammetric methods. The images from our new ground-based imager system showed to be valuable for validation of vertically thin cloud situations and for combination with satellite-based cloud boundaries to derive 3D cloud fields which can then be used for assimilation into numerical weather prediction and climate models.

In co-operation with Eumetsat, Free University of Berlin and RAL, the validation activities for satellite-based cloud height products will be continued. In addition to the geostationary satellites from the Meteosat First Generation (MFG), the data from Meteosat-8 will be used for CTW extraction and eventually stereo cloud-top height estimation in combination with Meteosat-5.

The ground-based photogrammetric validation activities will be continued with a stereo set-up of two operational Whole Sky Imagers at the ARM-SGP site, next to cloud radars, ceilometers and a Raman lidar.

ACKNOWLEDGEMENTS

The Meteosat-6/-7 data were received from the EUMETSAT Archive Facility (MARF), the ATSR2 data via the ESA ATSR2 NRT service, the AATSR data from the Rutherford Appleton Laboratory (RAL) and the EOS-Terra MISR data (level 1B2 and level 2TC) were obtained from the NASA Langley Research Center Atmospheric Sciences Data Center. This work is funded by the Bundesamt für Bildung und Wissenschaft (BBW) within the EU-projects CLOUDMAP (BBW Nr. 97.0370) and CLOUDMAP2 (BBW Nr. 00.0355-1) and by EUMETSAT within ITT-03/527.

REFERENCES

Baltsavias, E., 1991. Multiphoto Geometrically Constrained Matching. Ph.D. thesis, Institute of Geodesy and Photogrammetry, ETH Zurich, Switzerland, Mitteilungen Nr. 49.

Cloudmap2, 2004. Cloudmap 2 Final Report. EC 5th Framework Programme, Energy, Environment and Sustainable Development. To become available at http://www-research.ge.ucl.ac.uk/cloudmap2/publications.html

Diner, D., Davies, R., Di Girolamo, L., Horvath, A., Moroney, C., Muller, J.-P., Paradise, S., Wenkert, D., Zong, J., 1999. MISR Level 2 Cloud Detection and Classification. JPL Technical Report ATBD-MISR-07, Jet Propulsion Lab., California Inst. of Technol., Pasadena, CA, USA, available at http://eospso.gsfc.nasa.gov/eos_homepage/for_scientists/atbd/docs/MISR/atbd-misr-07.pdf (accessed April 30, 2004).

Eumetsat, 2003. Eumetsat homepage. http://www.eumetsat.de (accessed April 30, 2004).

Fischer, J., Preusker, R., Seiz, G., Poli, D., Gruen, A., Poulsen, C., Mutlow, C., Tjemkes, S., Borde, R., De Smet, A., 2004. Validation of cloud top pressure derived from MSG-SEVIRI observations through a comparison with independent observations. EUMETSAT Conference, Prague, 31 May-4 June.

Gruen, A., 1985. Adaptive least squares correlation: a powerful image matching technique. South African Journal of Photogrammetry, Remote Sensing and Cartography, 14(3), 175-187.

Gruen, A., Zhang L., 2002. Sensor modeling for aerial mobile mapping with Three-Line-Scanner (TLS) imagery. International Archives of Photogrammetry, Remote Sensing and SIS, Vol. 34, Part 2, pp.139-146.

Jovanovic, V., Bull, M., Smyth, M., Zong, J., 2002. MISR in-flight camera geometric model calibration and georectification performance. IEEE Transactions on Geoscience and Remote Sensing, 40(7), 1512-1519.

Jovanovic, V., 2004. MISR Level1 Quality Statement. http://eosweb.larc.nasa.gov/PRODOCS/misr/Quality_Summaries/L1_Products.html#registration (accessed April 30, 2004).

Lewicki, S., Chafin, B., Crean, K., Gluck, S., Miller, K., Paradise, S., 1999. MISR data products specifications. Technical report, NASA JPL, http://eosweb.larc.nasa.gov/PRODOCS/misr/readme/dps_ne_icd.pdf (accessed April 30, 2004).

Lorenz, D., 1985. On the feasibility of cloud stereoscopy and wind determination with the along-track scanning radiometer. Int. J. Rem. Sens., 6(8), 1445-1461.

Poli, D., 2003. Georeferencing of MOMS-02 and MISR stereo images with strict sensor model. ISPRS Workshop "High resolution mapping from space 2003", Hannover, October (on CD-ROM). Available at http://www.ipi.uni-hannover.de/html/publikationen/2003/workshop/contents.htm (accessed May 7, 2004).

Prata, A., Turner, P., 1997. Cloud-top height determination using ATSR data. Rem. Sens. Env., 59(1), 1-13.

Seiz, G., 2003. Ground- and satellite-based multi-view photogrammetric determination of 3D cloud geometry. Ph.D. thesis, Institute of Geodesy and Photogrammetry, ETH Zuerich, Switzerland, Mitteilungen Nr. 80.

Seiz, G., Baltsavias, E.P., Gruen, A., 2002. Cloud mapping from the ground: use of photogrammetric methods. Photogrammetric Engineering & Remote Sensing, 68 (9), 941-951.

Tjemkes, St., Lutz, H.-J., Duff, C., Watts, Ph., Poulsen, C., Wrench, Ch., Seiz, G., 2002. A multi-sensor analysis of cloud top pressure. EUMETSAT Users' Conference, Dublin, 2-6 September, Eumetsat Conference Proceedings, EUM P36.